JOURNAL OF SPACECRAFT AND ROCKETS
Vol. 36, No. 1, January–February 1999

Direct Simulation of Space Debris Evolution

Liqun Wang* and John P. W. Stark†
University of London, London, England E1 4NS, United Kingdom

The direct simulation Monte Carlo (DSMC) debris model has been developed at Queen Mary and Westfield College, University of London, and provides a statistical analysis to predict a long-term evolution of the orbital manufactured space debris environment with the aim to improve space vehicle risk assessment. This objective is achieved by assuming that debris can be modeled by employing sample particles to represent the real debris population. Based on the particle kinetic theory, the debris collision probability is evaluated rigorously. The combination of the breakup model, the collision probability model, and debris particle deorbit aerodynamic drag model leads to the debris population growth to be predicted. The DSMC debris model is validated by comparison with long-duration exposure facility impact experiments. Both time and ensemble statistics are used in the model for the Space Shuttle debris risk to be assessed and compared with the Shuttle window replacement data.

Nomenclature

a = orbit semimajor axis, km
B = ballistic coefficient, $m/(C_D\sigma)$, kg/m^2
C_D = air drag coefficient, 2.2
c = debris velocity, m/s
c_R = debris collision relative velocity, m/s
c_{Rmn} = collision relative velocity between debris components m and n, m/s
d = debris fragment size, m
E_p = projectile energy, J
e = orbit eccentricity
F_N = particle weighting factor
f = distribution function
f_1 = distribution function of another debris component
H = density scale height, km
i = orbit inclination, deg
M_e = ejecta mass, kg
M_f = fragment mass, kg
N = number of debris particles
N_{Cl} = number of collisions
N_{Cmn} = number of collisions between debris components m and n
N_{cum} = cumulative number of debris fragments
n = number density, km^{-3}
P = probability
$\boldsymbol{p}$ = debris population
Q = state variable
$\tilde{Q}$ = fluctuation of Q
$\bar{\tilde{Q}}$ = time average of $\tilde{Q}$
$\langle\tilde{Q}\rangle$ = ensemble average of $\tilde{Q}$
R = Earth radius, 6378.14 km
R_f = random function, $\in[0, 1]$
r = orbital object altitude, km
t = time, s
v_f = debris fragment velocity, m/s
v_r = debris relative collision velocity, km/s
ΔN_e = number of debris particles within $e \in [e_1, e_2]$
Δt = simulation time step, s
ΔV = simulation cell volume, m^3
θ = orbit true anomaly, deg
μ = Earth gravitational constant, 398,600 km^3/s^2
ρ = atmospheric density, kg/m^3
σ = cross-sectional area of orbital objects, m^2
σ_T = total cross-sectional area of two orbital objects, m^2
σ_{Tmn} = total collision cross-sectional area of orbital objects m and n, m^2
Ω = orbit right ascension of ascending nodes, deg
ω = orbit argument of perigee, deg

Subscripts

C = collision
c = circular orbit
cum = cumulative
f = fragment
m = particle index number m
n = particle index number n
p = perigee
R = solar radiation
0 = initial value

Received April 14, 1998; revision received Aug. 24, 1998; accepted for publication Aug. 26, 1998.

*Postdoctoral Research Assistant, Department of Engineering, Queen Mary and Westfield College.
†Professor and Head of Department, Department of Engineering, Queen Mary and Westfield College.

Introduction

SPACE debris is a large number of manufactured objects in space, such as spent satellites, upper stages, fragments of satellites and rocket stages, solid propellant particles, and paint flakes. The hazard to operational spacecraft posed by manufactured debris has become an important issue in recent years, as the collisions with the space debris have caused failure of a working satellite in addition to frequent Space Shuttle window replacement. This has resulted in the issue of both short- and long-term evolution of the space debris. The modeling and measurement of space debris are currently two parts of the debris studies. This paper concerns debris modeling and presents a novel approach, direct simulation Monte Carlo (DSMC) modeling, to model the space environment and achieve better understanding of the long-term evolution of space debris and its potential risk.

DSMC space debris modeling is a statistical approach. This is undertaken by employing sampled particles to represent the real space debris population.[1] The mathematical formulation of the DSMC method for multivariable analysis enables the debris DSMC model to be almost unrestricted in the complexity of the debris environment evolution that can be analyzed given sufficient computing power. It has been shown that this approach improves risk assessment by rigorously calculating collision frequency of the debris particles on the basis of particle kinetic theory. This has enabled us to look again at the evolution of the debris environment, in particular, to the generation of new debris from the existing debris environment. Debris evolution with fragmentation, followed by subsequent cascading, can be predicted if suitable corresponding models for these events can be provided.

The DSMC debris model is presented in detail. The model is verified by comparing results with the long-duration exposure

facility (LDEF) impact experimental data for microdebris and millimeter-size debris particles. LDEF was designed to provide long-term data on the space environment and its effects on space systems and operations. It successfully carried scientific and technology experiments that have revealed a broad and detailed collection of space environmental data. The debris collision probability and debris spatial flux are selected for this analysis. The evidence from the comparisons presented in this paper adds further credence to the validity of the DSMC model.

The Space Shuttle debris risk is assessed as an application of this model to debris risk analysis. Until July 1997, more than 52 windows of Space Shuttles have been replaced. The first collision avoidance maneuver was performed during STS-48 in September 1991. In Shuttle missions STS-72 to STS-94, in aggregate 162 days, 197 window pits were found and 16 windows were replaced. From our simulations, it is revealed that the collision rate between the Space Shuttle windows and microdebris ($\sim$40 μm) is very high.

Estimates of the future debris environment and the hazard caused by the future debris population growing are also of interest and concern in space debris research. Long-term debris evolution is simulated using the DSMC model. The simulated results show the steady increase in debris in the low-Earth-orbit (LEO) region if no mitigation measure is taken, even if no objects are launched into orbit.

DSMC Debris Model

Debris Particle Chaos

A major assumption in this study is that the space debris is in a chaotic state. The study of this debris chaos is through analysis of evolution of the orbital elements of a debris cloud produced by on-orbit breakup events. Our study has shown that, depending on size and altitude of generation, a breakup event will result in a random distribution in the argument of perigee and right ascension of ascending node on a timescale shorter than the lifetime of the clouds.[2] The space debris chaotic state assumption is, thus, justifiable, and the particle kinetic theory can be applied to DSMC debris study.

Particle Kinetic DSMC Modeling

Based on debris chaos, together with the assumption of only two object collisions (the result of the low density of debris), particle kinetic theory can be used. In DSMC modeling, a particle kinetic system is employed to represent the debris particle environment. The system is established by assigning each particle at time t a position and velocity. That is, for N particles in the system $\{\boldsymbol{r}_i, \boldsymbol{v}_i\}_t$, for $i = 1, 2, \ldots, N$, must be given. The evolution of the system is achieved by time marching with time step Δt. The evolved upgraded system state is replaced by $\{\boldsymbol{r}_i, \boldsymbol{v}_i\}_{t+\Delta t}$.

In particle kinetic theory, the evolution and behavior of the particle system is governed by the Boltzmann equation.[3] Therefore, the DSMC debris modeling is, in this sense, a modeling of the Boltzmann equation. Instead of trying to solve the equation by simplifying the equation so that analytic methods technique can be used, the DSMC scheme employs a particle transport scheme for direct numerical simulation.

To describe how the DSMC kinetic model solves the Boltzmann equation, we express the Boltzmann equation in the form of isolating the time derivative term as follows:

$$\frac{\partial(nf)}{\partial t} = \sigma_T \int_{-c\max}^{c\max} n^2 \Delta(ff_1) c_r \, \mathrm{d}\boldsymbol{c} - \boldsymbol{c} \cdot \nabla(nf) - \boldsymbol{F} \cdot \nabla'(nf) \tag{1}$$

Thus, the rate of change of the number of particles in phase space $\mathrm{d}\boldsymbol{r}\,\mathrm{d}\boldsymbol{c}$ is the sum of a term representing the convection of particles in physical space $\mathrm{d}\boldsymbol{r}$ and the convection of particles in velocity space $\mathrm{d}\boldsymbol{c}$ due to force $\boldsymbol{F}$ and the scattering of particles due to collisions.

This may be seen in the following way: In (nf), n is the particle number density and f is the particle velocity distribution function. In the Boltzmann equation, (nf) is the dependent variable and is equivalent to the system state variables $(\boldsymbol{r}_i, \boldsymbol{v}_i)$. That is,

$$(nf) \equiv (\boldsymbol{r}_i, \boldsymbol{v}_i) \tag{2}$$

In the DSMC particle modeling, $(\boldsymbol{r}_i, \boldsymbol{v}_i)$ for each particle i is assigned by an assumed distribution function of (nf).

Thus, the left-hand side of the equation is the time derivative of system state variables. For each time increment, three right-hand side terms require iteration: a collision term, a physical space term, and a velocity space term. The last two terms can be considered as one phase space terms. Therefore the Boltzmann equation, in this sense, is a time-dependent unsteady equation. However, this time dependence of the equation can be utilized numerically to solve both steady- and unsteady-state problems by a so-called time-marching scheme: a time-dependent solution leading to or converging to a time-marching solution in time steps. This is the final system state described by $(\boldsymbol{r}_i, \boldsymbol{v}_i)$.

Thus, in a typical DSMC particle scheme, within a time interval Δt, the following two steps are undertaken: 1) Particles are moved to correspond to the last two terms for particle convection in physical space, and 2) particles are collided with each other to correspond to the first term for changes of particle velocity distribution functions. In the DSMC particle scheme, we artificially decouple the two steps. This means we have to select carefully the time step Δt, typically of order one-third of the mean collision time. These two decoupled steps, particle moving and particle colliding, are repeated, and the system state is updated with time marching. As the modeling is stochastic, the state of the final system variables must be determined by statistical averaging, leading to either time averaging or ensemble averaging.

The process of particle movements in a rarefied gas (the principal application for DSMC) is trivial in that no external field of forces exists to accelerate particles. Modification of a particle velocity is, however, essential in debris analysis because the motion is governed by these forces, which act on orbital objects (in low Earth orbit principally gravity and aerodynamic drag). In the DSMC space debris modeling, the particle-move step must include an analytical expression for orbit propagation. In this scheme, instead of computing the trajectory of each particle, a stochastic orbital propagator, which will be soon given in detail, is used to assign each particle in its most probable location.

In the particle collision step, the debris particles collide with each other based on appropriate particle collision probability models. The postcollision properties are obtained based on debris in-orbit breakup models. The collision partner selection is random but based on particle kinetic theory. The particle collisions are undertaken in a frame of cells constructed in the LEO region so that only the particles that are in the same cell or near each other are allowed to collide.

Simulation Statistical Averages

The time-marching scheme toward final (not equilibrium) state system variables requires statistical averaging. In the DSMC scheme, two averages are used: ensemble and time averages.

The time average is established by summing the time-dependent properties of the debris particles in the simulation over an extended time interval. Suppose one of the system state variables of interest is to be at location r (some region in the Earth orbit) and is represented by Q (for example, debris density or debris flux, etc.) The value of Q fluctuates with time t, denoted by $\tilde{Q}$. The time-averaged value of $\tilde{Q}$, $\bar{\tilde{Q}}$ is then expressed as

$$\bar{\tilde{Q}} = \lim_{T \to \infty} \frac{1}{T} \int_0^{\infty} \tilde{Q}(r, t) \, \mathrm{d}t \tag{3}$$

This is realized by carrying out a long-time simulation to approach the statistical average.

The ensemble average is an instantaneous average of the simulation taken over the debris particles in the simulation domain in a large number of similar systems, for example, N experiments. The ensemble averaged solution can be established in two ways. The first formulation is a variation of the time averaging by taking N samples at different time steps t_n and then averaging the samples:

$$\langle \tilde{Q}(r, t) \rangle = \lim_{N \to \infty} \frac{1}{N} \sum_{n=1}^{N} \tilde{Q}(r, t_n) \tag{4}$$

The second formulation is by taking and averaging samples from N similar simulation systems, where each system runs for the same time duration t':

$$\langle \tilde{Q}(r, t') \rangle = \lim_{N \to \infty} \frac{1}{N} \sum_{n=1}^{N} \tilde{Q}_n(r, t') \tag{5}$$

This ensemble average can be realized by selecting a number of groups of different random numbers to establish different simulation systems. For the steady case, time averaging and ensemble averaging should lead to the same solution. In our study, we usually prefer the ensemble averaging to time averaging. In the long-term study, as applied to the LDEF impact study, we use the first formulation of the ensemble averaging. For shorter-term Shuttle debris risk analysis, we use the second ensemble averaging. For unsteady time-evolved debris evolution, for example, debris population growth prediction analysis, only the ensemble averaging of the second formulation can be used.

The following discusses in detail the particle moving and particle colliding routines.

Debris Particle Moving Routine

The debris convection in phase space is based on a debris orbital propagator. Each debris particle has its own orbit before interacting with another particle. Each sample debris particle in this space is expressed by six orbital elements (semimajor axis a, eccentricity e, true anomaly θ, inclination i, right ascension of ascending nodes Ω, and argument of perigee ω) evolved with time. These can then be used to identify the location of each particle at each time step.[4] The orbital elements change due to perturbations such as aerodynamic drag, the nonspherical Earth gravitational field, and lunisolar perturbations.

As mentioned earlier, a suitable time interval must be selected to achieve consistency between debris collision and debris convection. Although a small time interval is suitable for accurate debris tracking, a large time-interval value is chosen to achieve a consistent computation of the collision term due to the relatively low collision rate. Thus, instead of computing the trajectory of each particle, each debris particle is ascribed to its most probable location, based on a time-weighted residence.

Numerically, for a particle with altitude r and eccentricity e, the time spent in the altitude range Δr is calculated by

$$\Delta t = \sqrt{(p/\mu u)}\Delta r \tag{6}$$

where

$$u = e^2 - (p/r)^2 + (2p/r) - 1 \tag{7}$$

and

$$p = a(1 - e^2) \tag{8}$$

The probability is calculated as

$$P(r, e) = \Delta t / T \tag{9}$$

where T is the orbit period.

In practice, a table is made given time as a function of e and r, and a bilinear interpolation is conducted for each particle in the simulation to find its most probable location to enhance computational efficiency.

Debris Collision Probability Routine

The collision term is simulated by employing rigorous collision probability and collision dynamics schemes. The collision probability is a function of the debris particle collision cross-sectional area and the relative velocity.

The basic quantities associated with a debris model are debris size, mass, shape, orientation, and material of each debris particle. In this study, the debris shape is simply a sphere with diameter d. Other complex shapes can be adopted. The debris is composed of particles with a range of sizes. (Typical simulation is from a few micrometers to meters in extent.) For particles of different sizes (the so-called debris particle mixtures), we group particles by size in bins. Therefore, for two particles that are in groups m and n, the total cross-sectional area σ_{Tmn} for these is simply defined to be

$$\sigma_{Tmn} = \pi d_{mn}^2 \tag{10}$$

where

$$d_{mn} = \frac{d_m + d_n}{2} \tag{11}$$

and d_m and d_n are the diameters of particles of species m and n; m and n can range from 1 to s, where s is the number of species assumed to constitute the debris mixture.

Apart from particle grouping by sizes, another important numerical aspect in the DSMC debris modeling is selection of representative particles. These representative particles are to enable a few particles in the simulation to represent a much larger number of real particles, for example, one particle to represent F real particles, where F is defined as the weighting factor. This weighting factor must vary for particles of different sizes. This is particularly important in debris modeling due to the logarithmic-type distribution of the number of debris particles against the debris sizes. In reality, whereas there are only a few hundred large (satellite size) debris particles, there are millions of subcentimeter particles. Simulation error can be large if a single-valued weighting factor is applied to these different-size particles. Therefore, we use smaller values of F for large particles and large values of F for small particles. The detailed collision probability calculation is the following:

Consider a simulation domain divided into cells, with cell volume ΔV in which each simulated particle represents F real particles. Thus, the number of particles for components m and n are $F_m N_m$ and $F_n N_n$. The number of collisions N_{Cmn} during a time step Δt in cell volume ΔV between the component m particles and component n particles from kinetic theory is

$$N_{Cmn} = F_m N_m F_n N_n \langle c_{Rmn} \sigma_{Tmn} \rangle \Delta V \Delta t \tag{12}$$

where $\langle c_{Rmn} \sigma_{Tmn} \rangle$ represents the average value. Numerically, as in the collision routine, the number of collisions is calculated by summing over first all m ($m \in Z[1, s]$) and then all n ($n \in Z[1, s]$), where s is the total number of particle groups (components). This doubly counts the number of collisions, and to avoid this, we introduce a symmetry factor of one-half. This is reflected in the following calculations:

In theory, the number of collisions between component m particles and component n particles can be calculated. However, in a DSMC scheme, we always want to avoid calculating $\langle c_{Rmn} \sigma_{Tmn} \rangle$ because it involves doing a sum of $N_m N_n$ pairs of particles in the cell. We undertake a so-called acceptance/rejection scheme.[5]

The acceptance/rejection scheme is carried out in the following steps:

1) The maximum possible number of collisions between component m particles and component n particles is calculated as

$$(N_{Cmn})_{\max} = \tfrac{1}{2} F_m N_m F_n N_n (c_{Rmn} \sigma_{Tmn})_{\max} \Delta V \Delta t \tag{13}$$

2) A candidate pair of collision partners, i and j, is selected at random from particle component group m and n.

3) The relative velocity between particle i and j is calculated.

4) The collision probability P is calculated as

$$P = \frac{c_{Rmn} \sigma_{Tmn}}{(c_{Rmn} \sigma_{Tmn})_{\max}} \tag{14}$$

5) A random number R_f that satisfies $R_f \in [0, 1]$ and uniformly distributed within [0, 1] is calculated.

6) The candidate collision pair i and j is accepted as a collision partner to construct a collision event if

$$P \geq R_f \tag{15}$$

If the collision pair is accepted, a collision event is undertaken based on an in-orbit breakup model, as will be described. Then go to step 8.

7) The candidate collision pair i and j is rejected if

$$P < R_f \tag{16}$$

If the candidate collision pair is rejected, return to step 2 to choose another candidate collision pair.

8) Iterate by one the value of N_{Cmn}. Go to step 2 to choose the next candidate collision pair until

$$N_{Cmn} = (N_{Cmn})_{\max} \tag{17}$$

is satisfied.

The advantage of the DSMC scheme is obvious. First, particles of different sizes can be easily accommodated and grouped. Some debris models have difficulties in dealing with this debris mixture. Second, as this is a direct simulation, no assumed collision probability model, for example, Poisson model, is adopted a priori. Again some debris models require such a model to be adopted. This is a significant advantage of the direct simulation because preassumed collision rates are unreliable. Consequently, in the DSMC, the details of the collisions can be depicted as the averaged value of $\langle c_{Rmn}\sigma_{Tmn}\rangle$ actually simulated rather than just being guessed, as is the case in other debris models. Third, acceptance/rejection has very high computational efficiency.

Debris Collision Dynamics

A collision between two debris particles (above a certain threshold energy) creates more small debris particles depending on the nature of the collision (a function of collision cross section and relative velocity). The number, sizes, and velocities of the debris particles after collision can be determined only by using collision models usually obtained from representative experiments. In our debris modeling, it is assumed that the ejecta mass follows a power law and the remainder, if the collision energy is above a certain threshold energy, obeys an exponential law, as described in Ref. 6.

The use of the power law of Bess[7] determines the number and sizes of fragments after collision. The cumulative number of fragments N_{cum} can be expressed as

$$N_{\text{cum}} = k(M_f/M_e)^{-b} \tag{18}$$

where b is nominally taken to be 0.65 and k is determined by mass conservation. The postcollision velocity v_f is determined by

$$\log(v_f/v_r) = 0.225 - 0.1022[\log(d_f/d_{\min})]^2 \tag{19}$$

where $d_{\min} = E_p^{1/3}/6.194 \times 10^7$, where E_p is projectile energy.

The cumulative distribution function of an exponential law[8] has the following form:

$$N_{\text{cum}} = T M_b \exp\left(-UM_f^{\frac{1}{2}}\right) \tag{20}$$

The mass available for breakup, M_b, is the mass of the target minus the ejecta mass, T is an empirical constant (=0.0005), and U is determined by mass conservation. The postcollision velocity v_f is then obtained using[9]

$$\log v_f = -0.0676(\log d_f)^2 - 0.804\log d_f - 1.514 \tag{21}$$

Once the postcollision velocities have been determined, it is possible to calculate the orbital elements for the new debris distribution.

It should be noted that the power law predicts an unrealistically high number of small fragments. From our simulations, it is evident that the orbits of small fragments can be highly eccentric, with a very short lifetime due to a low perigee. As a result, the number of collisions generated from these is very small, and it is not felt that they significantly bias the overall collision frequency in the debris environment.

DSMC Astrodynamic Model

This section discusses the astrodynamic aspect of the DSMC debris model. As discussed in the preceding section, the first step of the DSMC method, particle convection routine, is associated with the debris particle motion. This is the orbital object propagator. The motion of orbital debris particles is dominated by the atmospheric drag, lunisolar perturbations, solar radiation pressure, and effects of the Earth gravitational field. Therefore, the motion of each orbital object is not Keplerian. Lagrange's perturbation theory can be applied to obtain an appropriate formulation. In our DSMC debris model, the noted perturbations are all taken into account.

Atmospheric Drag

The effect of aerodynamic drag is most notable for orbital objects under 1000 km and is progressively weaker up to 2000 km. It causes the semimajor axis a and eccentricity e to be changed. In LEO, aerodynamic drag retards debris particles at perigee, with a resulting reduced value of a and e. For debris particles with equal perigee, the lifetime of the particles with higher eccentricity values is longer. It has been shown that the collision between particles creates highly eccentric small-size particles even if the two colliding debris particles are in circular orbits. Orbital objects with lower ballistic coefficients [$B = m/(C_D\sigma_T)$] are most rapidly affected by the aerodynamic perturbation. Here, m is mass. Small debris particles have a lower ballistic coefficient. King-Hele's atmosphere/satellite interaction model[10] is employed and predicts changes in the semimajor axis a and eccentricity e.

For circular orbits, the change of semimajor axis per orbit is

$$\Delta a = H\,\ell_n\left(1 - \frac{2\pi\rho_c a_c^2}{BH}\right) \tag{22}$$

For eccentric orbits, the changes of semimajor axis a and eccentricity e per orbit are more complicated. The theory is developed in three parts, depending on the value of eccentricity ($0 < e < 0.02$, $0.02 < e < 0.2$, $e > 0.2$). For the full King-Hele theory, refer to Ref. 10.

Effects of the Solar Radiation Pressure Perturbation

Solar radiation pressure striking orbital objects causes periodic variations in the orbital elements. Its effect, like air drag, providing a surface force, has greater influence for orbital objects with lower ballistic coefficient (larger cross-sectional area and low mass). Therefore, objects such as small particles of a few grams or less (such as solid motor effuents) are mostly affected, inducing rapid decay, and, hence, are removed from the space environment. For average values of solar activity and objects below 800-km altitude, acceleration from atmospheric drag is greater than that from solar radiation pressure. Above 800 km, acceleration from solar radiation pressure is greater. The intensity of the solar radiation pressure in our DSMC model has been assumed to be constant, neglecting the small variation due to the Earth's orbit. The effect of the Earth's albedo has also been neglected as a first approximation. Eclipse variation has, however, been included.

In the DSMC debris model, the magnitude of acceleration a_R in meters per second squared from the solar radiation pressure is calculated as

$$a_R = -4.5 \times 10^8 \sigma/m \tag{23}$$

where σ is the cross-sectional area of orbital objects exposed to the sun in square meters and m is the mass of the orbital object in kilograms. Specular reflection surface is assumed. To calculate the changes of orbital elements due to the solar radiation pressure, the equations given by Cook[11] are used.

Lunisolar Perturbations

DSMC debris modeling adopts Cook's theory for the lunisolar (third-body) perturbation analysis. This was derived from Lagrange's planetary equations by integrating over one orbit revolution. In this theory,[11] it is assumed that the ratio of orbital object altitude height to the third disturbing body altitude height (r/r_d) is

taken as first order. This leads to the limitation of orbital objects whose semimajor axis does not exceed $\frac{1}{10}$th of the moon's distance from the Earth (equivalent to 38,440 km). Because the DSMC modeling is applied to LEO (altitude height $\leq$2000 km), this approximation is appropriate. The rates of changes of the orbital elements, i.e., semimajor axis, eccentricity, perigee height, inclination, argument of perigee, and right ascension of ascending nodes averaged over one revolution, are given by Cook.[11]

Effects of the Earth Gravitational Field

The Earth is appreciably oblate, and the effects of this are included via the perturbation due to J_2 alone. This results in migration of the right ascension of ascending node Ω and precession of the argument of perigee ω with time. The rates of change in degree per day of orbital elements are based on the following model given by King-Hele in Ref. 6:

Right ascension of ascending node:

$$\dot{\Omega} = -9.964(R/a)^{3.5}(1 - e^2)^{-2}\cos i \tag{24}$$

Argument of perigee:

$$\dot{\omega} = 4.982(R/a)^{3.5}(1 - e^2)^{-2}(5\cos^2 i - 1) \tag{25}$$

Debris Distribution Functions

These influences are fundamental to the chaotic debris assumption described earlier and dealt with in Ref. 2. The debris state vector can be established by assigning a position and velocity of each simulated particle. To combine the kinetic theory with astrodynamics, it is necessary to link the two using distribution functions for the six orbital elements: a, e, θ, i, Ω, and ω.

Suppose the fraction of debris particles of certain size that are located within an eccentricity interval Δe is ΔN_e and the total number of particles of this size is N. Then, the distribution function for eccentricity e can be given as

$$f_e = \Delta N_e / N \tag{26}$$

In our DSMC modeling, the simulated particles are generated from the distribution function f_e. A similar definition is used for the other orbital elements.

The debris distributions in our model were obtained from both empirical data and theoretical considerations. For trackable objects (~8000 objects larger than 10 cm), orbital element data are available from NASA two-line element data. Nontrackable objects do not necessarily follow the same distribution functions as the trackable objects. Because spacecraft are generally launched into orbit below 1100 km, the region between 1100 and 2000 km contains mostly breakup fragments and microdebris from the few large satellites. The eccentricity distribution is also quite different for debris of different sizes. Large particles follow circular or near circular orbits as observed, whereas small particles and fragments caused by the intercollisions between orbital objects are highly eccentric. Debris will largely retain the inclination at which it was produced. Evolution in inclination is predominantly as a result of lunisolar gravity. Below 800 km, aerodynamic drag will dominate over lunisolar effects. Again debris will largely retain the inclination at which it was produced because it is only slightly changed due to the aerodynamic drag. The inclination values are mostly populated from 60 to 110 deg with smaller peaks around 5 deg (not for LEO) and 28 deg. We assume that this is the case for both large objects and small fragments. Currently, because of the small changes expected, our model does not include evolution of inclination.

All other orbital elements (true anomaly, argument of perigee, and right ascension of ascending node) are assumed to be uniformly distributed for all debris sizes.

As new particles are created, the background debris particle distribution functions are perturbed. For instance, following a collision or explosion, the debris eccentricity distribution function will be updated with a large proportion of highly eccentric small particles. The perturbation of the eccentricity distribution of the debris population leads to changes in the debris velocity distribution. This then influences the collision rate. The effect of aerodynamic drag on this new particle distribution in eccentricity is then to evolve the orbit back to being more nearly circular over a period of time.

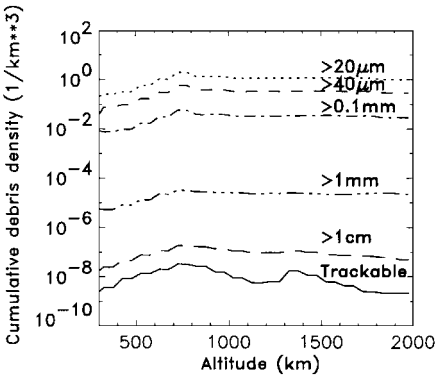

Fig. 1 Debris density distribution for debris sizes 20 μm, 40 μm, 0.1 mm, 1 mm, and 1 cm, and trackable objects.

As the initial debris distribution functions are based on a combination of empirical data together with the assumptions defined earlier, these distributions require updating during a simulation of the evolving environment. In the simulation process, the orbital elements of each object are sampled from other evolving orbital element distribution functions.

A typical case of the initial distributions for debris classified into groups based on sizes 20 μm, 40 μm, 0.1 mm, 1 mm, 1 cm, and trackable objects is shown in Fig. 1.

Simulation Domain

The DSMC debris simulation domain includes the LEO region up to an altitude of 2000 km. This then allows the debris particles from high orbit to decay, due to aerodynamic drag, into lower regions. To reflect a highly evolved debris environment, the simulation domain is divided into 40 subdomains, each representing a spherical 50-km shell, centered on the Earth. The analysis performed suggests that such an evolved structure will happen on a timescale short compared to the orbit decay timescale, and thus this assumption is valid for the type of study being undertaken. As the average mean collision time is approximately several days, the time step in the simulation is one day.

Comparison with LDEF Experiments

LDEF Structure

LDEF had a nearly cylindrical structure, and its 57 experiments were mounted in 86 trays about its periphery and at its two ends. It measured 30 ft (9.15 m long) $\times$ 14 ft (4.27 m in diameter) (~ cross section of 39 m^2). The total exposed surface area was 130 m^2 with 14 facing surfaces. The launch weight was 21,500 lb (9724 kg) with experiments.

LDEF Mission

LDEF was deployed in orbit on April 7, 1984, by the Space Shuttle Challenger. The nearly circular orbit was at an altitude of 257 n mile (476 km) and an inclination of 28.4 deg. LDEF remained in space for 5.78 years and completed 32,422 Earth orbits. It experienced one-half of a solar cycle, as it was deployed during a solar minimum and retrieved at a solar maximum. Its orbit had decayed to 179 n mile (331 km) when it was retrieved on Jan. 11, 1990, by the Space Shuttle Columbia.

LDEF Impact Data

The LDEF impact data from the Interplanetary Dust Experiment (IDE) were investigated by the Meteoroid and Debris Special Investigation (MDSI) group.

The IDE provided high-time-resolution detection of microparticle impacts on the LDEF satellite. Particles, in the diameter range from 0.2 μm to several hundred micrometers, were detected impacting on six orthogonal surfaces. As LDEF was gravity-gradient stabilized and magnetically damped, the direction of the normal to each detector panel is known for each impact. The results

from a nearly 12 months' tape-recorded data set represent the most extensive record gathered of the number, orbital location, and incidence direction for microparticle impacts in LEO. Because of high-resolution monitoring on board, the total number of recorded impacts between LDEF and microdebris is quite high. A total of 15,000 impacts were recorded on 459 detectors during the active phase of the mission (348 days).

Only one large (centimeter size) debris impact was recorded during the mission. This impact was spotted at the space end of LDEF at low-impact velocity.

The MDSI group documented and photographed more than 5000 visible impacts including craters (>500 μm) and penetrations (>300 μm) on LDEF surfaces during their inspection at Kennedy Space Center. These documented craters ranged in size from approximately 0.5 to 5 mm.

The experiments demonstrated the difficulties of distinguishing debris sources. Further investigations[12] suggested that about 80–85% of the craters were caused by meteoroids, leaving 15–20% to be caused by manufactured space debris. These percentage figures vary with direction of the impacting particle, with 25–30% on the leading edge and 10% on the trailing edge caused by debris.[13]

Simulation Conditions

It was assumed for the debris simulation that LDEF was kept at a mean altitude of 458 km. Debris collision frequency, flux, and impact velocity were evaluated and the simulated results compared with some corresponding LDEF experimental results.

The simulation uses the first formulation of the ensemble averaging, with 100 individual runs. The simulation enables identification of the debris flux and impact velocity.

As the LDEF experiment showed that most collisions are between LDEF and microdebris, the simulations concentrate on the interactions between LDEF and microdebris. Consequently, the simulated debris particles are binned into 10 groups based on their sizes: 20 μm, 40 μm, 65 μm, 0.1 mm, 0.24 mm, 1 mm, 1 cm, 10 cm, 3 m, and LDEF. Group 10 is specially for LDEF,[14] which is assumed to have an averaged effective diameter size of 7.0 m, with a collision cross section of 39 m^2 and exposure area of 133 m^2.

Simulation Results and Comparison with LDEF

Debris Flux

At the debris size lower limit, the collision probability routine of the DSMC model was compared with the LDEF flux data. Note that 65 μm was assumed to be the smallest particle size for producing a crater size larger than 500 μm. This particle size is about two to eight times smaller than that of the crater, depending on the collision incidence and impact velocity. Particles smaller than this size were used only for testing the flux routine of the model.

The spatial flux predicted in the simulation is plotted in Fig. 2 as square symbols for debris particle sizes 240, 100, 65, 40, and 20 μm. These flux data can be compared with the orbital debris flux data from the IDE analysis given by Simon et al.,[15] plotted as a solid line in Fig. 2. As the IDE data are given for debris size of up to 100 μm, a dashed line is used here for the IDE data to be extended to 240 μm for comparison with the DSMC results. This comparison shows that, for debris size larger than 40 and 65 μm, the DSMC prediction values are slightly higher than the IDE data. The predicted flux fit well for 20-μm and 0.1-mm debris with the IDE measurement. As a whole, the DSMC prediction agrees with the IDE measurement well.

Collision Frequency

Table 1 gives the simulated number of collisions between LDEF and different debris groups based on ensemble averages. It can be seen that the collisions between 0.1-mm or smaller debris particles and LDEF dominate the total number of collisions. For example, 660 and 2295 impacts by 0.1-mm and 65-μm particles are predicted for the life of the LDEF mission. This leads to collision rates of ~113 (0.1 mm) and ~396 (65 μm) collisions per year for LDEF by these microdebris.

A more critical way to compare LDEF data with the DSMC model is to evaluate which of the simulated collisions would produce a crater size greater than 500 μm, taking into account both the size and velocity of the impacting debris. The average value obtained over the 100 simulations was 783 impacts. As already noted, the analysis by MDSI documented 5000 craters of this size. The simulation results only calculate impacts due to manufactured debris. Thus, the ratio of our simulated impacts to observed impacts implies that 16% of the observed impacts should be due to debris, the remainder being due to natural environment effects. This percentage is in excellent agreement with the conclusions of Humes,[12] indicating that the manufactured debris accounted for between 15 and 20% of the impacts on LDEF.

The simulated collision rate between LDEF and larger debris particles is low, and this agrees with the LDEF postretrieval analysis that large craters are caused by natural debris. However, as the collision rate between LDEF and a 1-mm-sized debris particle is close to 0.1/year, the risk of an impact from a 1-mm manufactured debris is high. Based on the derived collision rate, a Poisson probability is then derived and is plotted in Fig. 3. This simulated collision rate (0.1/year) is indicated by the solid curve in Fig. 3. The simulated probability of no collision between LDEF and a 1-mm particle within 5.7 years is 56%. In other words, the simulated probability of having at least one collision is 44% within 5.7 years. This probability value may explain why there was a millimeter-size debris particle creating a 5.2-mm crater, the largest crater on LDEF.

Impact Velocity

From the LDEF postretrieval study, it was found that the majority of craters appeared to be the result of hypervelocity impacts with a velocity around 10 km/s. The DSMC model is able to sample the impact velocity distribution; this is plotted in Fig. 4. It is seen that the most probable impact velocity appears to be approximately 14 km/s, with the average impact velocity of 10.3 km/s. The lower average impact velocity is a consequence of a larger low-speed population of the velocity distribution function.

Table 1 Simulated collision frequency (impacts/year)

Group:	65 μm	0.1 mm	240 μm	1 mm	1 cm	3 m
LDEF	396	113	16	0.1	0.001	——

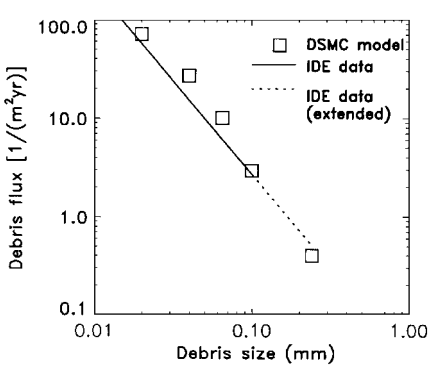

Fig. 2 Simulated debris flux data.

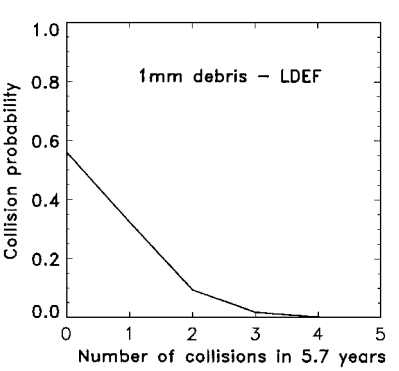

Fig. 3 Simulated collision probability.

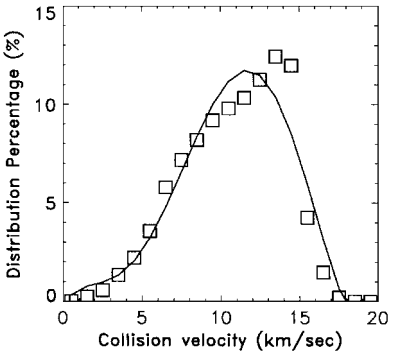

Fig. 4 Simulated debris impact velocity distribution on LDEF.

In accordance with the LDEF postretrieval investigation, the findings of impacts on the trailing end led to a prediction of the existence of the elliptical manufactured microdebris in orbit. As already indicated, the DSMC model employs a high eccentricity distribution function, and the simulated impacts on the trailing edge can be deduced as a logical consequence, due to the high velocity such particles have in the vicinity of perigee.

Space Shuttle Space Debris Risk Predictions

Shuttle Flight Risk due to Space Debris

Risk assessments are regularly made for missions such as that of the Space Shuttle. The first Shuttle windscreen was replaced in June 1983 after being chipped by a fleck of paint of about 0.3 mm and traveling at a speed of about 4 km/s on flight STS-7 (Challenger). Until July 1997, more than 52 Shuttle windows have been replaced. The first collision avoidance maneuver was performed during STS-48 in September 1991. In 13 Shuttle missions (STS-72 through STS-94), in aggregate 162 days, 197 window pits were found and 16 windows were replaced (no window pit data for STS-81 and STS-94).

The debris risk assessments are conducted by NASA for each preflight Space Shuttle mission. This risk assessment determines the relative risk of each proposed mission using the BUMPER model. The BUMPER model computes the probability of damage from debris and meteoroid particle impacts based on the Poisson statistical analysis from random events. When the assessment indicates that the mission profile results in risks outside the accepted limits, changes to the mission profile are analyzed until such time as an acceptable risk is achieved.

Space Shuttle window damage has been analyzed by Levin and Christiansen,[16] and their results are shown in Table 2 for Space Shuttle missions STS-72 through STS-94. According to Levin and Christiansen[16] and Levin et al.,[17] microdebris can cause a window pit, and a 40-μm or larger debris particle can cause the Shuttle window to require replacement. The damage listed in Table 2 is supposed to be caused by manufactured debris. From Table 2, we can see that the number of window replacements caused by microdebris is higher. It should be noted that an entirely new environmental model has been adopted by the BUMPER model since STS-80. It can be seen that the predictions have since been improved. It is also noted that the length of the mission is often different from that planned, and this has a significant impact on the number of debris impacts.

Shuttle Mission Debris Impact Data

It can be seen from Table 2 that the number of postflight windows replaced for each flight mission varies from zero to four. Mission duration varied from 8 to 18 days. The mission altitudes also varied from 278 to 463 km, with inclinations of 28, 39, and 52 deg.

Although the orbital parameters have a large range of variation, it is possible to perform a simplified statistical analysis based on various assumptions. First, assume that the window replacement is due to 40-μm-size debris particles striking the Shuttle windows. Second, for simplicity, the inclination difference and the altitude differences among the different missions are discounted. An overall average impact rate can then be calculated. From Table 3 and Fig. 5, it is found that the number of replacements varies between zero and four for each Shuttle mission. The most probable replacement is one window, with lesser probability of zero and two. There is, however, a lower chance for more windows to require replacement following a single mission. The mean value of the number of strikes is equal to 0.99 hit per day. This is roughly equivalent to one hit in seven to eight days. That is, on the average, one window must be replaced after each Shuttle mission.

Table 2 Shuttle window damages and BUMPER predictions

Shuttle mission	BUMPER prediction	Window replacement	Window pits	Duration, day	Orbit inclination	Average altitude, km
STS-73	1.21	2	8	15.91	39.0	278
STS-74	0.73	0	2	8.19	51.6	395
STS-72	0.3	0	0	8.92	28.45	463
STS-75	0.5	1	7	15.74	28.45	296
STS-76	0.7	1	20	9.22	51.6	296
STS-77	0.46	2	13	10.03	39.0	283
STS-78	0.3	1	2	16.91	39.0	278
STS-79	0.75	4	12	10.14	51.6	315
STS-80	0.42	2	31	17.66	28.45	351
STS-81	1.0	1	n/a	10.21	51.6	296
STS-82	0.9	0	23	9.98	28.45	579
STS-83	0.5	0	60	3.98	28.45	296
STS-84	0.7	1	19	9.22	51.6	296
STS-94	0.7	1	n/a	15.70	28.45	296

Table 3 Shuttle window damage statistical analysis

Number of window replacements	Frequency			
	$i = 28.45$ deg	$i = 39$ deg	$i = 51.6$ deg	All i
0	3	0	1	4
1	2	1	3	6
2	1	2	0	3
3	0	0	0	0
4	0	0	1	1
Total strikes (postflight)	4	5	7	16
Mission, days	71.98	42.85	46.98	161.81
Replacement rate[a]				
Postflight	0.056	0.117	0.149	0.099

[a]Strike/day.

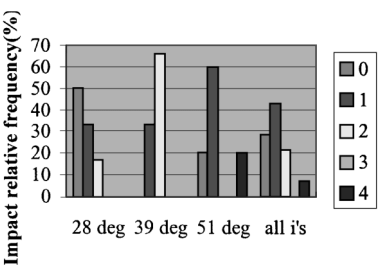

Fig. 5 Impact frequency (based on Shuttle postflight data).

Modeling Space Shuttle Debris Risk Assessments

In the DSMC simulation, we take a typical Shuttle orbiter configuration with the dimensions length 37.24 m, wingspan 23.79 m, and height 17.25 m. The total exposed area is 1480 m^2, and the exposed window area is about 3.7 m^2.

In this simulation, we take a 40-μm impact to be the cause of the window replacement. In each simulation, the Shuttle flight altitudes are based on an individual flight datum from Table 2 and are between 300 and 400 km. The orbits are circular.

This DSMC Space Shuttle debris risk assessment can be simulated using either ensemble or time averages. The time average is obtained by simulating the debris collision process over a long period of time, typically in hundreds of days, to derive the mean collision rate of strikes per mission (as in the earlier LDEF simulation). However, from this type of simulation, it is not easy to see the randomness or fluctuation in the simulated data. Ensemble averaging enables simulated data to be established, which demonstrate these fluctuations. It was, therefore, this statistical average that was used in this Shuttle debris risk simulation.

Table 4 Simulated window replacement frequency

Number of window replacements	Frequency: Sample size = 100, $i = 28.45$ deg	Sample size = 100, $i = 39$ deg	Sample size = 100, $i = 51.6$ deg	Sample size = 300, all i
0	30	28	27	85
1	30	31	32	93
2	27	27	26	80
3	7	10	11	28
4	6	4	3	13
5	0	0	1	1
Sample mean	1.29	1.31	1.34	1.31
Impact rate[a]				
Simulation	0.107	0.109	0.112	0.11
Postflight	0.056	0.117	0.149	0.099

[a]Strike/day.

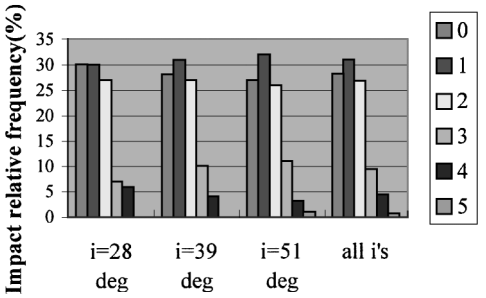

Fig. 6 Impact frequency (based on DSMC modeling).

In the analysis, we treat each simulation as a simulation of an unsteady transient process. We select three test cases for the three different typical inclinations: 28, 39, and 51 deg. For each case, we perform 100 simulations to find out how many 40-μm particles strike the Shuttle window in each simulation. Each simulation is for a 12-day mission. First, the number of debris particles striking the Shuttle window in the 100 simulations for each inclination case is obtained. Next, the frequency with which each value (the number of strikes) occurs is found. This frequency is listed in Table 4 and plotted in the bar chart of Fig. 6, where the height of each column is proportional to the frequency with which the value occurs for the three inclination cases individually. The bar chart of frequency makes it easier to see the general pattern of the discrete data.

From Table 4 and Fig. 6, it is found that the simulated number of window replacements, as in the real Shuttle mission, varies between zero and five within the 12-day Shuttle mission. However, we expect that it is more likely to be one window requiring replacement, with lesser probability of no window and two windows needing replacement. The probability of more than two window replacements is even lower. From Table 4, we can also calculate the mean value of the number of strikes, which is equal to 0.11 strike per day. This is roughly equivalent to one hit in seven to eight days.

We emphasize that this DSMC Space Shuttle debris risk assessment combines both ensemble and time averages. The time average is established by summing the appropriate properties of debris particles in the simulation over an extended time interval. This is realized by carrying out a long-time simulation to get a statistical average. The ensemble averages are instantaneous averages taken over the debris particles in the simulation domain in a large number of similar systems. This ensemble average can be realized by selecting a number of groups of different random numbers to establish different simulation systems.

Debris Population Growth

Artificial space debris has been continuously created since the first satellite was launched. As this population grows from various sources such as mission related objects, e.g., rocket bodies, upper-stage breakups, satellite breakup, and debris self-collisions, operating satellites are at risk due to random collisions with this debris background. The current way in which debris is cleansed from the LEO (altitude up to 2000 km) environment is as a result of aerodynamic drag and solar radiation pressure. Debris can remain in orbit, however, for hundreds of years. One of the main concerns is clearly future debris population.[18]

As analytical study of the population growth is usually based on an input–output principle: population growth = input − output. Ignoring launches, this leads to

$$\frac{\mathrm{d}\boldsymbol{p}}{\mathrm{d}t} = (K - C)\boldsymbol{p} \tag{27}$$

For multicomponent debris population analysis, we have

$$\boldsymbol{p}(t) = [p_1(t), p_2(t), \ldots, p_s(t)] \tag{28}$$

$$K = K(\boldsymbol{p}, t) \tag{29}$$

$$C = C(\boldsymbol{p}, t) \tag{30}$$

where s is the total number of debris components (groups), t is time, $p_i(t)$ is population at time t for debris component i, K is a proportionate debris production rate, and C is a proportionate debris decay rate, with both K and C being functions of debris population $\boldsymbol{p}$. Furthermore, here all variables are also functions of altitude.

If these functions can be established, the population growth can be predicted analytically. The value of $(K - C)$ is, however, difficult to determine. Although some analytical expressions have been introduced, the complexity of the debris interactions means that analytic expressions are too simple to describe the reality. Therefore, in this study, we adopt the DSMC debris model to perform the long-term prediction.

Simulation Conditions

Again, the simulation domain is the LEO region. In the simulation, it is assumed that the debris particle source term is from only one source: debris fragmentation. We are attempting to highlight the effect of self-collision within the debris environment. The detail of an individual traffic model, which will of itself also create additional debris, will make analysis more complex. Also, our predicted simulation will provide a minimum for any observed growth rate in the debris spatial density and flux. The fragment spatial density distribution in LEO up to 2000 km is shown in Fig. 7 (Ref. 19), classified into six groups based on size: 0.1 mm, 1 mm, 1 cm, 10 cm, 1 m, and 3 m. This is the debris fragment number density distribution function used in this simulation.

The simulation is for the debris population prediction of the next 25 years, which is shorter than the lifetime for much of the orbital debris in LEO. For example, a millimeter-size fragment with eccentricity 0.01 produced just above 700 km has a lifetime of 25 years. If its eccentricity is 0.1, the lifetime would be 400 years. A centimeter-size fragment with eccentricity 0.1 would not decay from perigee altitude of above 500 km within the 25-year simulation period.

As noted, the simulations do not include any new launches of satellites into orbit and merely reflect what would happen if the only

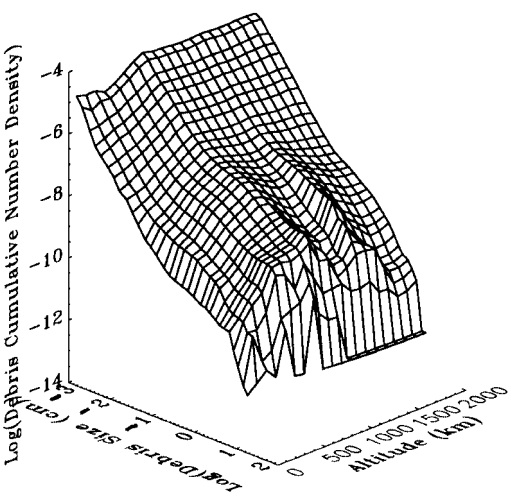

Fig. 7 Debris fragment density–altitude.

source of additional debris is as a result of collisions taking place within the current environment. This excludes any explosions from within the current population and will, thus, be an underestimate for debris number density.

Simulation Results

The simulation includes as many experiments as possible to form an ensemble statistics; each experiment employs 470,000 representative particles.

Based on the assumptions just discussed, the ensemble statistical debris population prediction result is shown in Fig. 8 as the population against time for fragments larger than 0.1 mm. Figure 8 shows both increasing population due to the breakup events and decreasing population due to the debris decay in certain time periods. From Fig. 9, it can be seen that the phase of the solar cycle influences the particle decay process. It can be seen that particles have a higher decay rate in solar maximum years 2001 and 2012 and a lower decay rate in solar minimum years 1996, 2007, and 2018. It is apparent that there is a near steady population with an increasing trend for fragments of all sizes. Detailed analysis reveals that fragments have different population growth rates for different sizes and in different regions.

Figure 10 demonstrates the dependency of fragment growth rate for different sizes in different regions. The highest growth rate in

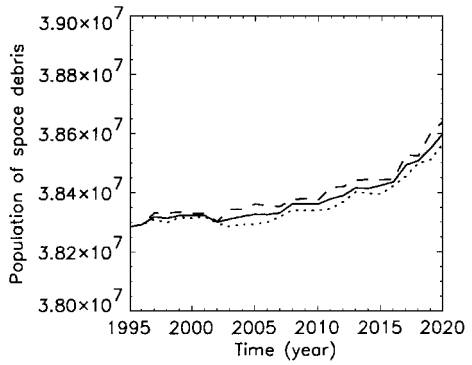

Fig. 8 Debris fragment population prediction from ensemble averages.

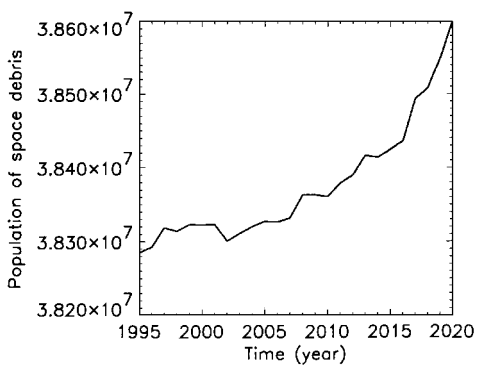

Fig. 9 Debris fragment population prediction from single simulation.

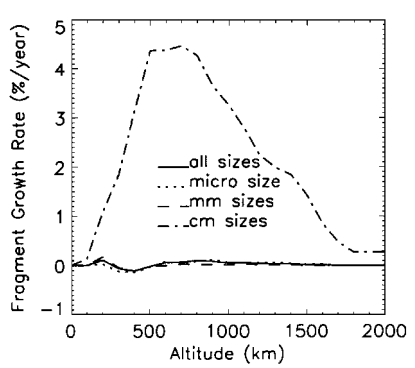

Fig. 10 Debris fragment growth rate.

number of fragments is in the altitude range just above 800 km. The region below 300 km is a very uncertain area with fragment population either increasing or decreasing in the simulation due to the stronger aerodynamic drag effect. It is expected that at the lowest altitudes (typically below 300 km) our simulation procedure is less accurate because the debris lifetime will be comparable to the orbital evolution lifetime. Thus, any new debris created below this altitude will not evolve to the chaotic state required for our basic model assumptions.

As far as the fragment size is concerned, the centimeter-size fragments have a much faster growth rate than others. The maximal growth rate at about 800-km altitude is around 5% per year, compared with the growth rate of smaller-size fragments of only around 0.3–1% per year.

In the simulation, as would be anticipated, the impacts for space systems mostly arise between large objects and number-dominating small particles (0.01–1 cm), creating more small fragments. The number of large particles does not increase because these would be caused by rare catastrophic events from in-orbit collisions between large objects. The production of large-debris objects from launch activities has been excluded in the simulation reported here, but it should be noted that the traffic model assumptions will have a significant influence on the evolution of the large-object population. Explosions are also excluded in the simulations. Collision probability increases with the increasing number of small-debris fragments. These impacts will control the future debris environment, having a most significant effect on the deterioration of spacecraft surfaces.

Typically, as mentioned earlier, the probability of a collision between two large objects is low. However, the simulation reveals a few collisions between objects larger than 1 cm, which could produce catastrophic damage. Although the number of fragments created from this type of collision is also a function of relative velocity, a relatively larger number of fragments are produced when this type of collision takes place. These can be noted from Fig. 9, which shows results for a single simulation in which the debris population grows significantly when a 3-m object collides with a 10-cm object, during the year 2012.

Conclusions

A novel approach to the space debris modeling problem, DSMC debris modeling, is successfully applied.

The validation of the DSMC modeling is shown from the analysis in which the DSMC model predicts collision frequency data that are consistent with the observed LDEF impact data.

The success of the DSMC model has led us to undertake Space Shuttle risk assessments and to predict long-term debris population growth. The model will be used for further debris study, including debris collision cascading.

In the Shuttle Orbiter risk analysis, we infer that the Shuttle window replacement rate is approximately one window per mission. This rate is compared with recent Shuttle window replacement data.

The dynamic DSMC predicts that the debris population will grow in the next century even without additional launches. More serious is that the centimeter-size debris fragment population will grow much faster than that of millimeter and micrometer fragments, increasing potential risk of catastrophic breakup of future satellites.

DSMC modeling, although reliable in practice, is complex in application, requiring significant computation resources. Nevertheless, the advantage of DSMC over other approaches lies in the way that collisions can be modeled from an appropriate statistical method.

Acknowledgment

This work was supported by the Engineering and Physical Science Research Council under agreement GR/J73636.

References

[1] Stark, J. P. W., "Direct Monte-Carlo Simulation of Orbital Debris," *Proceedings of 19th Rarefied Gas Dynamics* (Oxford, England, UK), Oxford Univ. Press, Oxford, England, UK, 1994, pp. 1373–1379.

[2] Stark, J. P. W., and Wood, N., "Chaotic Study of Space Debris" (manuscript in preparation).

[3]Bird, G. A., *Molecular Dynamics and Direct Simulations of Gas Flows*, Oxford Univ. Press, Oxford, England, UK, 1994.

[4]Fortescue, P., and Stark, J. P. W., *Spacecraft System Engineering*, Wiley, Chichester, England, UK, 1991, Chap. 4.

[5]Wang, L., Stark, J. P. W., and Crowther, R., "Direct Monte-Carlo Simulation of Collision Frequency of Orbital Debris," 46th International Astronautical Federation Congress, International Academy of Astronautics Paper 95-IAA.6.4.02, Oslo, Norway, Oct. 1995.

[6]McKnight, D. S., "Determination of Break-Up Initial Conditions," *Journal of Spacecraft and Rockets*, Vol. 28, No. 4, 1991, pp. 470–477.

[7]Bess, T. D., "Mass Distribution of Orbiting Man-Made Space Debris," NASA TN-D8108, 1975.

[8]McKnight, D. S., Maher, R., and Nagl, L., "Refined Algorithm for Structure Breakup Due to Hypervelocity Impact," Hypervelocity Impact Society Symposium, Sante Fe, NM, Oct. 1994.

[9]Reynolds, R., "A Review of Orbital Debris Environment Modelling at NASA/JSC," AIAA Paper 90-1355, 1990.

[10]King-Hele, D. G., *Satellite Orbits in an Atmosphere: Theory and Application*, Blackie, Glasgow, Scotland, UK, 1987, Chaps. 4–6.

[11]Cook, G. E., "Luni-Solar Perturbations of the Orbit of an Earth Satellite," *Royal Geophysical Journal of the Royal Astronomical Society*, Vol. 6, No. 1, 1996, pp. 271–291.

[12]Humes, D. H., "Small Craters on the Meteoroids and Space Debris Impact Experiments," *Proceedings of the 3rd LDEF Post-Retrieval Symposium: LDEF 69 Months in Orbit*, NASA CP-3275, Pt. 1, 1995, pp. 287–322.

[13]Zhang, J. C., and Kessler, D., "Orbital Debris and Meteoroid Population as Estimated from LDEF Impact Data," *Proceedings of the 3rd LDEF Post-Retrieval Symposium: LDEF 69 Months in Orbit*, NASA CP-3275, Pt. 1, 1995, pp. 373–384.

[14]Wang, L., and Stark, J. P. W., "Direct Simulation of Space Debris and Comparison with LDEF Impact Experiment," *Proceedings of 2nd European Conference on Space Debris*, ESA-SP-393, European Space Agency, 1997, pp. 333–338.

[15]Simon, C. G., Mulholland, J. D., Oliver, J. P., Cooke, W. J., and Kassel, P. C., "Long-Term Microparticle Flux Variability Induced by Comparison of Interplanetary Dust Experiment (IDE) Timed Impacts for LDEF's First Year in Orbit with Impact Data for the Entire 5.77-Year Orbital Lifetime," *Proceedings of the 2nd LDEF Post-Retrieval Symposium: LDEF 69 Months in Orbit*, NASA CP-3194, Pt. 2, 1993, pp. 693–703.

[16]Levin, G. M., and Christiansen, E. L., "The Space Shuttle Program: Preflight Meteoroid and Orbital Debris Risk/Damage Predictions and Post-Flight Damage Assessments," *Proceedings of 2nd European Conference on Space Debris*, ESA-SP-393, European Space Agency, 1997, pp. 633–636.

[17]Levin, G. M., Christiansen, E. L., Loftus, J. P., Jr., and Bernard, R., "Recent Results from Space Shuttle Meteoroid/Orbital Debris Pre-Flight Risk and Post-Flight Damage Assessments," 48th International Astronautical Federation Congress, International Academy of Astronautics Paper 97-IAA.6.4.01, Turin, Italy, 1997.

[18]Wang, L., and Stark, J. P. W., "DSMC Prediction of the Population Growth of the Space Debris," *Rarefied Gas Dynamics 20* (Beijing, PRC), Peking Univ. Press, Beijing, PRC, 1996, pp. 233–238.

[19]Spencer, D. B., Maethner, S. R., Yates, K. W., and Madler, R. A., "Program DEEP: A Modelling Approach for Estimating the Space Debris Environment and Its Effects," 46th International Astronautical Federation Congress, International Academy of Astronautics Paper 95-6.4.04, Oslo, Norway, 1995.

I. D. Boyd
Associate Editor